



Screen-Printable Contacts for Industrial *N*-TOPCon Crystalline Silicon Solar Cells

Meijun Lu, Kurt R. Mikeska , Chaoying Ni , Yong Zhao, Feibiao Chen, Xianqing Xie, Yawen Xu, and Changgen Zhang

Abstract—Optimally prepared industrial *n*-type bifacial tunnel oxide passivated contacts c-Si solar cells (156×156 mm) fabricated with cost effective screen-printable front-side (FS) and rear-side (RS) silver pastes had a median solar cell efficiency of $22.21\% \pm 0.10\%$ and bifaciality efficiency factor of 82.9%. A FS paste comprising silver, metallic aluminum, and inorganic frit was designed to contact p^+ boron-diffused Si emitter surfaces with $\text{SiN}_x\text{:H}$ - Al_2O_3 antireflection-passivation layers. A RS paste comprising silver and inorganic frit was designed to contact n^+ phosphorous-doped surfaces with tunnel- SiO_x/n^+ poly-Si/ $\text{SiN}_x\text{:H}$ layers. The bifacial electrical data indicates efficiency is being limited by the FS contact. The final FS bulk silver metal region microstructure shows isolated metallic aluminum particles surrounded by solidified liquid phase within the bulk sintered silver conductor line. The FS silver metal- p^+ boron-diffused emitter contact region shows continuous interfacial (IF) films decorated with silver colloids located between the bulk silver metal and emitter surface. The final RS silver metal- n^+ phosphorus diffused contact region again shows continuous IF films between the bulk silver metal and semiconductor surface. A microstructural model suggests electrical contact for both the FS and RS contact regions occurs by a tunneling mechanism though the residual IF films.

Index Terms—Bifacial, frit, metallization, *n*-type, paste, photovoltaic cells, screen print, silicon, solar cells, thick-film, tunnel oxide passivated contacts (TOPCon).

I. INTRODUCTION

TUNNEL oxide passivated contacts (TOPCon) cell technology has become the leading next-generation choice after mono PERC (passivated emitter and rear cell). Compared to technologies such as heterojunction technology and interdigitated back contact, TOPCon architectures can be achieved by

Manuscript received September 29, 2021; revised November 13, 2021 and December 11, 2021; accepted December 17, 2021. Date of publication January 13, 2022; date of current version February 19, 2022. (Corresponding author: Kurt R. Mikeska.)

Meijun Lu, Kurt R. Mikeska, Yawen Xu, and Changgen Zhang are with the Jiangxi Jiayin Science and Technology Company LTD, Nanchang 330013, China (e-mail: cynthia.lu@jxjiayin.cn; mikeskkr@gmail.com; xuyawen@jxjiayin.cn; zhangchanggen@jxjiayin.cn).

Chaoying Ni and Yong Zhao are with the Department of Materials Science and Engineering, University of Delaware, Newark, DE 19716 USA (e-mail: cni@udel.edu; yongzhao@udel.edu).

Feibiao Chen is with the College of Chemistry and Chemical Engineering, Jiangxi Normal University, Nanchang 330027, China (e-mail: chenfeibiao@jxjiayin.cn).

Xianqing Xie is with the Research Center of Carbohydrate Synthesis, Jiangxi Normal University, Nanchang 330027, China (e-mail: xiexianqing@jxjygd.com).

Color versions of one or more figures in this article are available at <https://doi.org/10.1109/JPHOTOV.2021.3138248>.

Digital Object Identifier 10.1109/JPHOTOV.2021.3138248

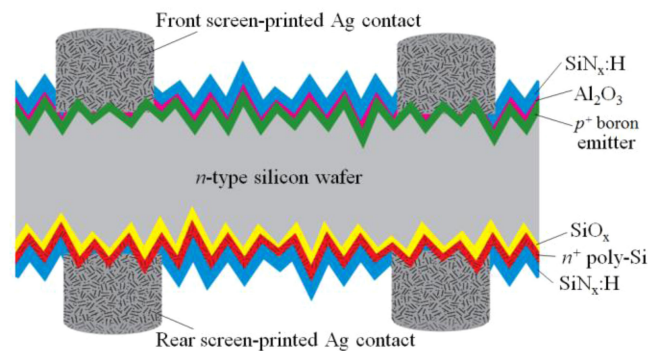


Fig. 1. Industrial *n*-TOPCon c-Si solar cell with front-side and rear-side screen-printed silver conductor lines.

upgrading current industrial PERC or PERT (passivated emitter rear totally diffused) manufacturing lines which means a lower capital expenditure is needed for existing PERC or PERT manufacturers who want to upgrade their existing production lines. We investigated *n*-type TOPCon since *n*-type silicon wafers have inherent advantages over *p*-type silicon such as higher minority carrier diffusion length and less sensitivity to metal impurities, and *n*-type cells do not have boron–oxygen-related light-induced degradation [1]–[3]. A TOPCon structure offers a gain in cell efficiency of $\sim 1\%$ absolute compared to previous generation technologies [4], [5].

Industrial cell manufactures utilize screen-printable pastes as a cost-effective metallization solution because of their low cost, high throughput, and relatively high performance. Previous generation pastes have been successfully designed to contact either n^+ -type emitters, in the case of *p*-type cells, or p^+ -type emitters, in the case of *n*-type cells. Among the challenges for introducing a TOPCon architecture to industrial solar cell manufacturing is designing and utilizing cost effective screen-printable pastes that effectively contact both the front-side (FS) and rear-side (RS) surfaces of the solar cell in a single paste firing step while maintaining the benefits of the TOPCon architecture [6].

We explore both FS and RS state-of-the-art screen-printable silver conductor pastes on an industrial *n*-type TOPCon bifacial structure shown in Fig. 1. It has an FS p^+ boron diffused emitter and an RS n^+ phosphorus diffused passivating contact, with screen-printed silver conductor lines on both the front and rear sides to obtain bifaciality. Each surface presents unique paste development challenges. The front surface requires a paste optimized for contact to a p^+ doped surface, the rear surface

requires a paste optimized for contact to a n^+ doped surface, all the while minimizing damage to the passivation layers.

Previously, we reported on electrical properties and FS contact region microstructure features of screen-printed industrial bifacial n -type TOPCon solar cells [7]. In this article, we further explore electrical properties, specifically FS and RS specific contact resistivity and conductor line resistivity, investigate the RS contact region microstructure, compare FS and RS microstructural features, and discuss contact mechanisms based on the microstructural features of the FS and RS. The chemical reactions that occur during the firing process in the FS and RS contact regions are also elucidated. This is the first time the chemistry and final fired microstructure of pastes designed to contact the FS and RSs of an industrial n -TOPCon solar cell are discussed.

II. EXPERIMENTAL

Screen-printable pastes were prepared by mixing silver metal powder (~ 90 wt%), inorganic frit powder (~ 2 wt%), and organic media (~ 8 wt%) in a planetary mixer followed by three-roll milling and viscosity adjustment (measured by a Brookfield DV2T-HB). Pastes were roll milled to a fineness of grind of ~ 5 μm in accordance with ASTM Test Method D 1210-05. Pastes were adjusted to a final viscosity between 150 and 450 Pa-s at 10 rpm.

Paste solar cell performance was evaluated on commercially available vendor supplied industrial processed bifacial n -type TOPCon mono c-Si pseudo-square (156×156 mm) random pyramid solar cells. The cell fabrication process included alkali texturing, p^+ boron diffusion (BBR_3), rear p^+ removal (single side HF/HNO_3 etching), rear thermally deposited SiO_x layer (~ 1.5 nm thick) and intrinsic poly-Si layer (low pressure CVD, 30 nm thick), n^+ phosphorus diffusion (POCl_3), front n^+ removal (single-side etching), front ALD- Al_2O_3 layer (atomic layer deposition, 5 nm thick), and double-sided $\text{SiN}_x\text{:H}$ deposition (plasma enhanced CVD, 70 nm thick). The final wafers had FS and RS sheet resistances of 80 Ω/sq and 40–50 Ω/sq , respectively. For the metallization, an industrial Baccini screen printer was used to print rear and front surface five busbar H-patterned conductor lines. The fired FS conductor line mean width was ~ 30 μm and height ~ 15 μm . The fired RS line mean width was ~ 50 μm and height ~ 12 μm . An industrial nine-zone Despatch furnace was used to fire the screen-printed wafers in a single step. The final screen-printed n -TOPCon cell configuration is shown in Fig. 1.

An industrial Berger I - V tester was used to measure solar cell efficiency (Eff), fill factor (FF), open circuit voltage (V_{OC}), short-circuit current (J_{SC}), and series resistance (R_s). Electrical data are median and standard deviation values for about 10 cells. Specific contact resistivity (ρ_c) was measured using the transmission line (or transfer length) method (TLM) [8] on 1.0 cm wide strips cut from fired cells. ρ_c data are median and standard deviation values for 50 TLM measurements. For the RS ρ_c measurement, which is a n^+ on n -wafer structure, some of the current during the TLM measurement will flow into the n -wafer, so not all the current is confined with the n^+ doped poly-Si layer.

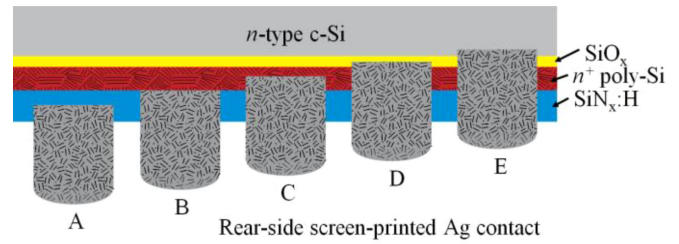


Fig. 2. Rear-side schematic showing possible contact scenarios.

To investigate this effect, the TOPCon cell vendor supplied us with bare n^+ on n -wafers and n^+ on p -wafers. In our article, the ρ_c of the n^+ on p -wafer is about twice the ρ_c of the n^+ on n -wafer. Theoretically, the n^+ on p -wafer is a more accurate ρ_c value. Hence, the RS ρ_c value for the TOPCon solar cell was corrected (multiplied) by a factor of two. This may not be completely accurate, but the RS ρ_c value is quite small, so the accuracy of the correction has only a minimal effect on the conclusions. Gibbs free energy (ΔG) values were determined using FactSageTM [9]. The chemical reaction equations are written with the same number of oxygen atoms in order to compare ΔG values among equations. Microstructure sample preparation and characterization was performed on an Auriga 60 CrossBeam (FIB/FE-SEM).

III. RESULTS AND DISCUSSION

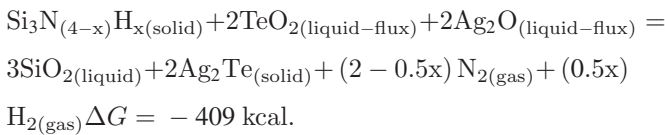
The challenge for pastes printed on the front and rear surfaces of a bifacial TOPCon structure is making electrical contact on both surfaces during the paste firing process without damaging the contact area under the silver conductor lines, which can increase the J_0 recombination current density and reduce the final solar cell V_{OC} . Ideally, the paste etches through the $\text{SiN}_x\text{:H}$ antireflective (ARC) layers on both the FS and RSs, which are electrically insulating and then stops, leaving the underlying layers undamaged. In practice, precise control of the etch-through process is quite difficult. Fig. 2 is a schematic drawing showing various etch-through and contact scenarios on the RS of the n -TOPCon structure. Fig. 2B is the ideal contact scenario. In Fig. 2B, the paste etches through the $\text{SiN}_x\text{:H}$ layer and stops at the n^+ poly-Si layer optimizing both ρ_c and J_0 . 2B is ideal but challenging to achieve in practice; and 2C is more practical. The other scenarios are not ideal. 2A will result in high ρ_c since $\text{SiN}_x\text{:H}$ etch-through is incomplete. 2D and 2E will result in damage to the passivation layers, especially in 2E where the paste etches through the passivation layers and into the underlying c-Si substrate. Similar contact scenarios can be envisioned for the FS where ideally etch-through removes the $\text{SiN}_x\text{:H}$ ARC and stops at the underlying emitter or passivation layer. To characterize the contact region details of an actual solar cell, it requires viewing the contact region in cross-section using electron microscopy, which is done in this article.

A thick-film, screen-printable paste typically consists of an organic phase, metallic silver particles, and an inorganic solid-state frit. The paste is printed on the wafer surface and rapidly fired at relatively high temperature ($\sim 730^\circ\text{C}$ – 780°C). During the firing process, the frit forms a liquid-phase flux that helps sinter the silver particles to high bulk density and etches through

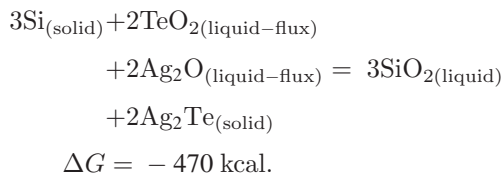
the electrically insulating $\text{SiN}_x\text{:H}$ ARC to allow the sintered silver conductor line to make electrical contact to the underlying surface, ideally without damaging the surface. Ideally, in a TOPCon structure, the RS tunnel oxide passivation layers would be left intact under the conductor lines. Sintering the silver particles to high density reduces conductor line resistance which reduces solar cell R_s . Effective contact minimizes the contact resistance which again reduces R_s . Contact to the underlying surface without damage to the surface reduces J_0 recombination in the contact region which increases V_{OC} .

The approach taken in this article was to design pastes to contact the doped surface (either n^+ or p^+). Screen-printable pastes designed to contact n^+ surfaces currently contain telluride-based frits [10]. These pastes are relatively well established as FS pastes for p -type base wafers with n^+ front emitters. Pastes designed to contact p^+ surfaces are less well established and usually contain aluminum metal particle additions to accomplish contact, but which suffer high emitter damage and relatively high contact resistance and high conductor line resistance compared to pastes for n^+ surfaces. Surface passivation layers on a TOPCon structure (on both FS and RS) further complicate contact. The ability of the paste to selectively etch the $\text{SiN}_x\text{:H}$ ARC and then contact the underlying passivation layers and doped surfaces without damage is possible but uncertain.

The RS paste was designed to make electrical contact to a phosphorous doped n^+ surface. It contained silver metal and a lead telluride (Pb-Te-O) based frit. Pastes with telluride-based frits are typically applied to the FS of p -type cells with n^+ front emitters. Applying a paste with a telluride-based frit to the RS of an n -TOPCon structure is unique and has not previously been discussed. Telluride-based frits form a liquid phase flux during the firing process that contain tellurium oxide and soluble metal ions such as silver, which dissolve and etch-through the $\text{SiN}_x\text{:H}$ ARC layer according to the following redox reaction [11]:



The large negative ΔG of reaction is thermodynamically extremely favorable. The removal of the $\text{SiN}_x\text{:H}$ layer allows the silver conductor line to make electrical contact with the underlying n^+ surface. Note that the dissolution process does not stop once the $\text{SiN}_x\text{:H}$ layer has been removed. The dissolution process will continue into the underlying Si substrate:



The FS paste was designed to contact boron doped p^+ surfaces. It contained silver metal, a lead-silicate (Pb-Si-O) based frit, and aluminum (Al) metal particles. Metallic Al is required to contact p^+ surfaces. The Al metal is thought to promote electrical contact by reacting with and penetrating into the p^+

TABLE I
SCREEN-PRINTED *n*-TOPCON CELL JV DATA

	Eff (%)	FF (%)	V_{OC} (mV)	J_{SC} (mA/cm ²)	R_s (m Ω)
FS Median	22.21 \pm 0.10	79.48 \pm 0.40	673.6 \pm 1.5	41.48 \pm 0.07	3.02 \pm 0.15
FS Best Cell	22.28	79.73	674.0	41.46	2.98
RS Median	18.41 \pm 0.18	79.27 \pm 0.50	667.9 \pm 1.4	34.77 \pm 0.21	3.52 \pm 0.35
RS Best Cell	18.58	79.71	669.0	34.84	3.07

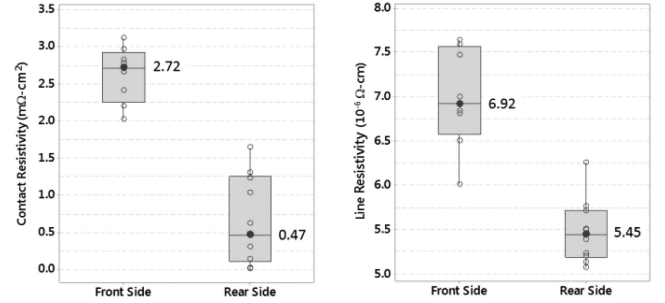
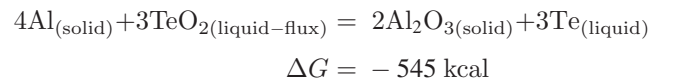


Fig. 3. Specific contact resistivity and silver conductor line resistivity of the front- and rear-sides of an industrial n -TOPCon cell.

doped Si surface during the firing process [12]. Both frit and Al metal are usually required in a paste for good contact. Paste comprising frit sans Al metal or comprising Al metal sans frit were tested and both resulted in solar cells with high ρ_C and poor JV values (Eff < 1%). Our experiments showed that Al metal additions cannot be used in pastes to contact n^+ doped surfaces since Al ions are a p^+ dopant and shunt paths on n^+ surfaces resulting in poor solar cell electrical performance. Our experiments also showed that telluride-based frits perform poorly in p^+ contacting pastes containing Al metal particles. This is because telluride frits strongly oxidize the surface of the Al metal particle during the firing process according to the following reaction:



rendering the Al particle inactive in the contact process. The large negative ΔG of reaction is extremely favorable.

Table I lists JV data for industrial n -TOPCon bifacial cells printed with FS and RS pastes showing median and “Best Cell” values for the FS and RS of the cells. The bifacial cells had an FS median Eff of 22.21 \pm 0.10% and a maximum Best Cell Eff of 22.28%, and an RS median Eff of 18.41 \pm 0.18% and maximum Best Cell Eff of 18.58%. The median bifaciality Eff factor is 82.9% according to the ratio of the RS illumination efficiency to the FS illumination efficiency (Eff_{rear}/Eff_{front}). Since the front and rear sides have similar V_{OC} and FF, the bifaciality Eff factor is comparable to the bifaciality J_{SC} factor ($J_{SC\text{-rear}}/J_{SC\text{-front}} = 83.8\%$).

Fig. 3 shows specific contact resistivity and conductor line resistivity comparing the FS and RSs of an n -TOPCon cell. The FS had a median ρ_C of 2.72 \pm 0.38 m Ω -cm². The RS had a median ρ_C of 0.47 \pm 0.60 m Ω -cm². The FS ρ_C value is a factor of \sim 5.8 higher than the RS ρ_C value. The RS ρ_C

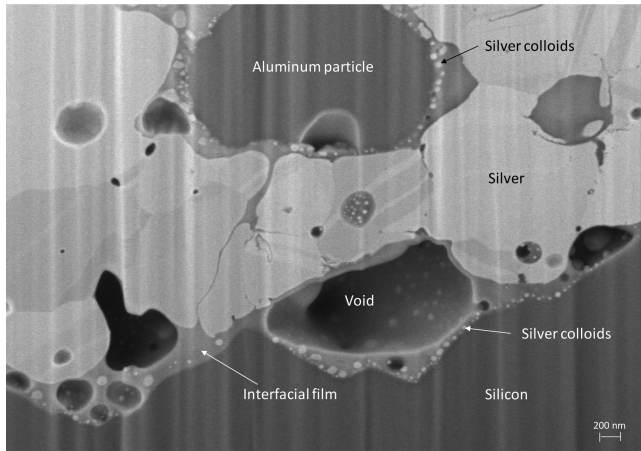
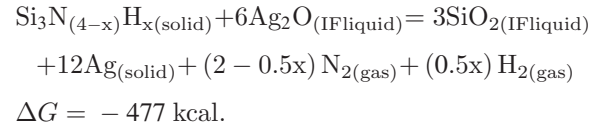


Fig. 4. SEM cross-section micrograph of the final front-side fire-through metallization contact region.

value is comparable to state-of-the-art screen-printable pastes designed for contact to phosphorous doped surfaces [12]. The FS ρ_C is quite high for an industrial solar cell. A ρ_C of $<1 \text{ m}\Omega\text{-cm}^2$ is preferred for low solar cell R_s and high FF. The contact resistivity data indicates a need to improve the FS contact. In addition to a need to improve FS contact, Al metal in the FS paste increases conductor line resistivity compared to the RS conductor line resistivity, as shown in Fig 3. The contact and line resistivity data indicate solar cell performance is being limited by the FS contact. Cell performance can be further improved if the FS contact can be optimized. Additional limiting factors are the relatively low FS and RS V_{OC} values. Aluminum metal in the FS paste exacerbates surface damage during firing under the FS conductor lines which increases J_0 recombination under the FS conductor lines which reduces FS V_{OC} . Also, as will be discussed, the RS contact region shows Ag crystallites decorating the RS contact interface which contribute to an increase in J_0 recombination under the RS conductor lines which reduces RS V_{OC} . Improvements in the RS passivation and base wafer quality can also improve cell performance.

Fig. 4 is an SEM micrograph of the FS contact region. The FS has a boron doped p^+ emitter coated with an Al_2O_x passivation layer and $\text{SiN}_x\text{:H}$ ARC. The light contrast area (top portion) is the sintered bulk silver conductor metal and the dark area (bottom portion) is the bulk silicon emitter. An interfacial (IF) film is observed at the interface between the bulk silver metal and silicon emitter. During the paste firing process, the inorganic frit in the paste forms a low viscosity liquid phase which migrates to the silver-silicon interface region where it enables the oxidation, dissolution, and removal of the $\text{SiN}_x\text{:H}$ layer resulting in IF films between the bulk silver metal and underlayer emitter. The IF films are inhomogeneous (chemically and physically) composites of reaction products from the dissolution of the $\text{SiN}_x\text{:H}$ layer by the liquid phase flux. Our considerable experience characterizing contact region IF films shows the films can be crystalline, semi-crystalline, and quite inhomogeneous depending on the starting frit chemistry, solar cell firing time/temperature profile, and film location and thickness along the IF region. Our preference is to call them IF films. In this case, the final IF film is decorated with silver

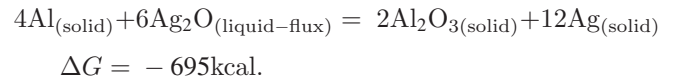
colloids from precipitation of silver ions dissolved in the IF liquid phase according to the following reaction:



It is not surprising to observe silver colloids considering the large negative ΔG of reaction.

A microstructural model suggests the silver colloids participate in electrical contact between the emitter and bulk silver by a tunneling mechanism through the IF film during cell operation and is consistent with current screen-printable paste contact models [13], [14]. The microscopy observation shows the IF film to be ubiquitous and continuous along the interface with no directed contact between the bulk silver and emitter layer. If direct contact does occur, it is intermittent and spotty, and not within the observed area, although our microscopy observations show no evidence of direct contact. The $\text{SiN}_x\text{:H}$ layer appears to be dissolved/removed along the interface. It is beyond the resolution of the SEM image to determine if the Al_2O_3 passivation layer has been removed. Silver crystallites are not observed along the interface.

Voids, pockets of solidified liquid, and a metallic Al particle are observed in the bulk silver metal. EDS analysis, not shown here for brevity, indicates the particle is aluminum metal. The aluminum particle is surrounded by solidified liquid-phase decorated with silver colloids that form during firing according to the following reaction from silver ions dissolved in the liquid phase flux:



It is not surprising to observe silver colloids surrounding the Al particle considering the large negative ΔG value. The isolated Al metal particle is not in contact with the surrounding bulk silver; therefore, it does not contribute to electrical conduction and increases conductor line resistance, as shown in Fig. 2, since Al is inherently less conductive than Ag. Metallic Al particles and/or Si–Al eutectic reaction products are not observed directly along the interface or in direct contact with the emitter surface. If these do occur, they are sporadic and outside the cross-sectional viewing area or they may occur at firing temperatures different from this article. Silver crystallites are not observed along the interface.

Fig. 5 is an SEM micrograph of the RS contact region. The RS has a passivating phosphorus doped SiO_x/n^+ poly-Si stack coated with $\text{SiN}_x\text{:H}$. Again, during the paste firing process, the liquid phase frit in the paste migrates to the silver- $\text{SiN}_x\text{:H}$ interface where the flux dissolves the $\text{SiN}_x\text{:H}$ layer. A continuous IF film is, again, observed along the contact interface. A proliferation of silver crystallites decorates the interface. Silver crystallites grow epitaxially into the Si $\langle 111 \rangle$ surface during the firing process and can penetrate relatively deep (many 10 s of nanometers) into the Si surface, depending on the paste firing conditions, and damage the underlying silicon surface resulting in a J_0 reduction under the metallization [15]. In this case,

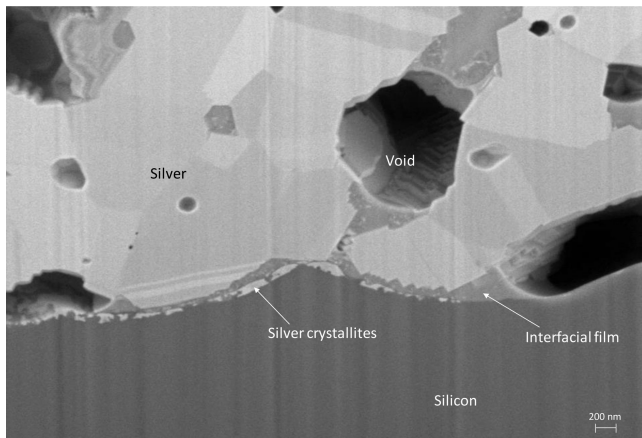


Fig. 5. SEM cross-section micrograph of the final rear-side fire-through metallization contact region.

the abundance of crystallites along the interface indicates the crystallites have penetrated the SiO_x/n^+ -poly-Si stack and have grown epitaxially into underlying the Si wafer surface. The crystallites also have an IF film located between the crystallites and bulk silver metal. The crystallites do not appear to make direct contact with the bulk silver metal. For pastes containing tellurite-based frits designed to contact phosphorus diffused surfaces, as employed in this article, silver crystallites in the contact region indicate an over fired condition. An ideal contact interface has no crystallites. The RS microstructural features suggest electrical contact between the semiconductor surface and bulk silver metal occurs by a tunneling mechanism through the IF film. It is beyond the resolution of the SEM image to determine if the tunnel- SiO_x/n^+ -poly-Si stack has been dissolved during the firing process, but the abundance of crystallites along the interface indicates the stack has been penetrated.

Both the FS and RS contact regions appear to have continuous IF films located between the bulk silver metal and semiconductor surfaces, although the detailed microstructural features are different for each side. A microstructural model suggests electrical contact for both the front and rear contact regions occurs by a tunneling mechanism through the residual IF films.

This has been an initial investigation (i.e., first-attempt) to design and apply a screen-printable paste comprising a telluride frit to the RS and a paste comprising metallic aluminum and a lead-silicate frit to the FS of an industrial *n*-TOPCon solar cell. Additional performance gains can be achieved by further optimizing the paste time/temperature firing profile to maximize both the front and RS electrical properties, and/or adjusting the front and RS paste chemistries (i.e., frit chemistries) to more fully optimize etch-through and contact. Further insights can also be gained through high-resolution TEM characterization of the contact region, which was not done here since this was a “first attempt.”

IV. CONCLUSION

In the development of an industrial *n*-type TOPCon solar cell, cost-effective FS and RS screen-printable silver pastes were investigated resulting in a median bifacial cell efficiency of $22.21 \pm 0.10\%$ and a maximum efficiency of 22.28% . The bifacial

electrical data indicates efficiency is being limited by the FS contact. The final FS microstructure shows isolated metallic aluminum particles surrounded by solidified liquid within the bulk sintered silver conductor line. The FS silver metal- p^+ boron-diffused emitter contact region shows continuous IF films decorated with silver colloids located between the bulk silver conductor metal and emitter surface. The final RS silver metal- n^+ phosphorus diffused contact region also shows continuous IF films located along the interface between the bulk silver conductor metal and semiconductor surface. Silver crystallites decorate the RS semiconductor surface.

Solar cell performance can be further improved if the FS contact can be optimized. Additional limiting factors are the relatively low FS and RS V_{OC} values. Aluminum metal in the FS paste exacerbates surface damage during firing under the FS conductor lines which increases J_0 recombination under the FS conductor lines which reduces FS V_{OC} . Silver crystallites along the RS contact interface contribute to an increase in J_0 recombination under the RS conductor lines which reduces RS V_{OC} .

A microstructural model suggests electrical contact for both the front and RS contact regions occurs by a tunneling mechanism through the residual IF films.

REFERENCES

- [1] J. Benick, B. Hoex, M. C. M. van de Sanden, W. M. M. Kessels, O. Schultz, and S. W. Glunz, “High efficiency n-type Si solar cells on Al_2O_3 -passivated boron emitters,” *Appl. Phys. Lett.*, vol. 92, no. 25, Jun. 2008, Art. no. 253504.
- [2] A. Edler, “Development of bifacial n-type solar cells for industrial application,” Ph.D. dissertation, Univ. Konstanz, Konstanz, Germany, Dec. 2014.
- [3] J. Schmidt and K. Bothe, “Structure and transformation of the metastable boron- and oxygen-related defect center in crystalline silicon,” *Phys. Rev. B*, vol. 69, no. 2, Jan. 2004, Art. no. 024107.
- [4] F. Feldmann, M. Bivour, C. Reichel, H. Steinkemper, M. Hermle, and S. W. Glunz, “Tunnel oxide passivated contacts as an alternative to partial rear contacts,” *Sol. Energy Mater. Sol. Cells*, vol. 131, pp. 46–50, Dec. 2014.
- [5] F. Feldmann, M. Simon, M. Bivour, C. Reichel, M. Hermle, and S. W. Glunz, “Efficient carrier-selective p- and n-contacts for Si solar cells,” *Sol. Energy Mater. Sol. Cells*, vol. 131, pp. 100–104, Dec. 2014.
- [6] D. Chen et al., “24.58% total area efficiency of screen-printed, large area industrial silicon solar cells with the tunnel oxide passivated contacts (i-TOPCon) design,” *Sol. Energy Mater. Sol. Cells*, vol. 206, Mar. 2020, Art. no. 110258.
- [7] M. Lu et al., “Screen-printable conductor metallizations for industrial n-TOPCon crystalline silicon solar cells,” in *Proc. 48th IEEE Photovolt. Specialists Conf.*, 2021, pp. 0954–0957.
- [8] D. K. Schroder and D. L. Meier, “Solar cell contact resistance—A review,” *IEEE Trans. Electron. Devices*, vol. 31, no. 5, pp. 637–647, May 1984.
- [9] C. W. Bale et al., “FactSage thermochemical software and databases, 2010–2016,” *Calphad*, vol. 5, pp. 35–53, Sep. 2016.
- [10] A. F. Carroll, K. W. Hang, B. J. Laughlin, K. R. Mikeska, C. Torardi, and P. D. VerNooy, “Thick-film pastes containing lead- and tellurium-oxides, and their use in the manufacture of semiconductor devices,” U.S. Patent 8497420 B2, Jul. 30, 2013.
- [11] K. R. Mikeska, M. Lu, and W. Liao, “Tellurium-based screen-printable conductor metallizations for crystalline silicon solar cells,” *Prog. Photovolt. Res. Appl.*, vol. 27, no. 12, pp. 1071–1080, Aug. 2019.
- [12] W. Wua, K. E. Roelofs, S. Subramoney, K. G. Lloyd, and L. Zhang, “Role of aluminum in silver paste contact to boron-doped silicon emitters,” *AIP Adv.*, vol. 7, no. 1, Jan. 2017, Art. no. 015306.
- [13] Z. R. Li, L. Liang, and L. K. Cheng, “Electron microscopy study of front-side Ag contact in crystalline Si solar cells,” *J. Appl. Phys.*, vol. 105, no. 6, Mar. 2009, Art. no. 066102.
- [14] Z. G. Li et al., “Microstructural characterization of front-side Ag contact of crystalline Si solar cells with lightly doped emitter,” in *Proc. 38th IEEE Photovolt. Specialists Conf.*, 2012, pp. 002196–002199.
- [15] D. Inns, “Understanding metal induced recombination losses in silicon solar cells with screen printed silver contacts,” *Energy Procedia*, vol. 98, pp. 23–29, Nov. 2016.